CHAPTER II

THEORY AND LITERATURE REVIEW

This chapter describes the theoretical and application aspects of track etched detector, neutron interaction, theory of light as well as literature review.

2.1 Principles of Track etched detector

2.1.1 Mechanism of Track formation

A complete satisfactory model of track registration and formation mechanisms does not yet exist. There are many models to explain the process of track formation. The **"Ion Explosion spike model"** [3] is so for the most reasonable theory (Figure 2.1). According to this model a positively charged energetic particle passing through a medium knocks out the orbital electrons of atoms lying in and around the vicinity of its passage. The dominant process is the ionization of K or L shell electrons. Due to this knock out of electrons a cylindrical region full of positive ions (holes) is produced. Due to Coulomb repulsion between positive charged ions some of them are ejected into the interstitial positions leaving behind a vacancy rich and a few microns long (40-80 A^{o}) cylindrical core. In view of this model track formation mechanism depends upon a variety of parameters, such as mass, ionization state and velocity of the incident ion and ionization potential of the absorbing material. In the case of electrical conductors and good semi-conductors the electrons around this region neutralize the cylindrical region of positive holes so that such media are not able to register the passage of incoming ions. While in crystalline solids these positive ions thereupon repel one another violently, thus disturbing and distorting the regular lattice in crystal produce a more or less cylindrical region (30 A^{o}) under a high strain[6].

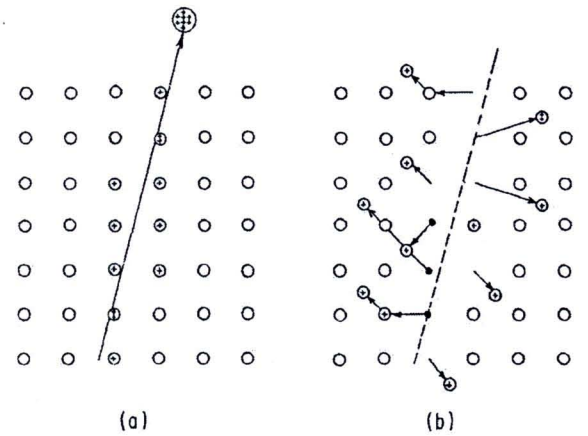

Figure 2.1 The ion explosion spike mechanism for track formation in inorganic solids. The original ionization left by passage of a charged particle (a) is unstable and ejects ions into the solid, creating vacancies and interstitials (b). [3]

The ion explosion spike model requires the following conditions for track formation.

a) The electrostatic stress must be greater than the bonding strength of the crystal. This shows the material of low mechanical strength or low dielectric constant is more likely to store etchable tracks.

b) There must be at least one ionization event per atomic place for the track formation to be automatically continuous.

c) The free electron density of the track storing material must not be greater than a permissible maximum value. This condition restricts track formation in good insulators alone and thus metals do not store tracks.

d) The hole mobility of material must not be high because this results into neutralization of the core atoms which in turn will prevent the formation of track. Thus semi-conductors like silicon and germanium having high hole mobility will not form tracks.

In organic polymers the traversing ion breaks the long molecular chains and produces relatively stable free radicals, small gas inclusion and other products of chemical radiation damage, by ionization and excitation of primary particles and δ-ray, shown as Figure 2.2. Broken chains ends & free radicals are produced in this region. The density of the absorbing material is reduced in this region, which has been directly

observed by low energy neutron scattering. These new region are latent damaged trails and can be seen at very high magnification (30,000x) under a transmission electron microscope [7].

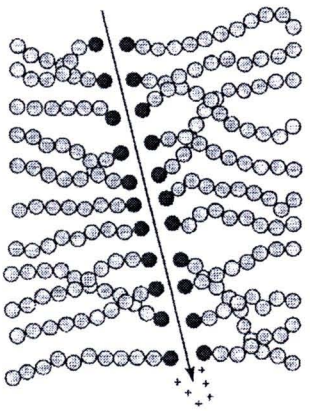

Figure 2.2 Schematic illustration of a chain scission in polymers caused by the passage of heavily charged particles. [8]

2.1.2 Restricted energy loss [1, 9]

The primary process of charged-particle interaction with the detector material is ionization and excitation of the molecules in the detector. The initial charged particle loses its energy through the many interaction processes. Theoretically, it interacts through Coulomb force with charged particles (electrons and nuclei) in the material. Of course, distal interactions may be neglected and we focus on the particle interactions with atoms and molecules that are close to its path. The majority of the interactions occur with electrons and only a small number of interactions are with nuclei. Since the initial heavy charged particle (only such particles can produce tracks) is much heavier than electrons, the direction of the particle effectively does not change and the path is almost completely a straight line. This may not be true if the particle interacts with a nucleus, where a significant deviation from the initial direction may occur. However, such interactions are relatively rare. Some deviations from the straight line can happen close to the end of the particle range, when the energy of a particle becomes very low.

The particle loses its energy in many small interaction processes, so the energy loss each time is usually very small when compared to its energy. For example, ionization of one molecule in air on average needs about 32 eV, which is 10^{-5} to 10^{-6} of the particle energy (assuming that the particle energy is in the MeV region). As a result of these many

small interaction processes, the particle will continuously slow down in the detector material. The physical quantity that describes the slowing down of charged particles in mater is the stopping power -dE/dx (or the stopping force used by some authors), where dE is the energy lost in the distance dx. Stopping power is given in J/m or in keV/mm. The energy lost by a particle in the distance dx is the energy transferred to the material so this quantity is also called the linear energy transfer (LET).

Stopping power is proportional to the square of the charge of the incoming particle, Z_1^2, and it is inversely proportional to its velocity; thus the stopping power increases as the particle velocity is decreased.

The classical formula that describes the specific energy loss is known as the Bethe-Bloch Formula, which is valid for all types of heavy charged particles with velocities that are large compared to orbital electron velocities.

The Bethe-Bloch formula has different forms for heavy and light particles:

- For heavy charged particles (α particles and protons):

$$-\frac{dE}{dx} = \frac{4\pi Z^2 e^4}{m_e \upsilon^2} NB$$

$$B = Z\left[\ln\frac{2m_e\upsilon^2}{\mathrm{I}} - \ln\left(1-\frac{\upsilon^2}{c^2}\right) - \frac{\upsilon^2}{c^2}\right] \qquad (2.1)$$

where υ is velocity of the charged particle

Ze is charge of the charged particle

N is number density of the target

M_e is rest mass of the electron

I is experimentally evaluated average excitation and ionization potential

B is stopping number

- For light charged particles (electrons and positrons)

$$-\frac{dE}{dx} = \frac{2\pi e^4}{m_e \upsilon^2} NB$$

$$B = \left[\ln\frac{m_e\upsilon^2 E}{2\mathrm{I}^2(1-\beta^2)} - (\ln 2)\left(\sqrt{1-\beta^2} - 1 + \beta^2\right) + 1 - \beta^2 + \frac{1}{8}\left(1-\sqrt{1-\beta^2}\right)^2\right] \qquad (2.2)$$

$\beta = \upsilon/c$

For the charged particles with $\upsilon << c$ (non-relativistic particles) only the first term in the stopping number (B) equation is necessary. Equations 2.1 and 2.2 show that B varies slowly with particle energy and is proportional to the atomic number (Z) of the absorber material. Thus the stopping power varies as $1/\upsilon^2$, or inversely with particle energy.

The Bethe-Bloch formula also shows that higher-Z materials have greater stopping powers. Table 2.1 demonstrated I values of various compounds.

Table 2.1 Mean ionization/ excitation potential I for various compounds [10]

Compound	I (eV)	Compound	I (eV)
Air (dry)	85.7	Lithium fluoride	94
Water (liquid)	75	Photographic emulsion	331
Water (vapor)	71.6	Sodium iodide	452
Muscle (skeletal)	75.3	Polystyrene	68.7
Bone (compact)	91.9	A-150 plastic	65.1

2.1.3 Range-Energy relationship [9]

The general expression for linear stopping power (linear energy loss) for a charged particle that is slowing down in a medium is the Bethe-Bloch formula. Since the energy loss is proportional to the square of the charge of the coming particle, an α particle is expected to stop much faster than a proton in a given medium.

Semi=empirical formulas express the range of charge particles as a function of kinetic energy.

For α particles, the range in air at a temperature of 15°C and 760 mm pressure is given by the equations

$$R_{air}(cm) = \begin{cases} 0.56\left(\frac{cm}{MeV}\right)E(MeV) & E\langle 4MeV \\ 1.24\left(\frac{cm}{MeV}\right)E(MeV) - 2.62(cm) & 4MeV\langle E\langle 8MeV \end{cases} \quad (2.3)$$

The range (expressed as density thickness) of an α particles in any other medium, R_m, is given by

$$R_m(cm) = \frac{0.00056A^{1/3}}{\rho_m} R_{air} \quad (2.4)$$

where A is the atomic mass number of the medium, R_{air} is the range of the α particles in air, and ρ_m is the density of the medium.

The proton range in air is defined as

$$R_{air}(m) = \left[\frac{E_p(MeV)}{9.3}\right]^{1.8} \quad for \quad E_p\,(few\,MeV - 200MeV) \tag{2.5}$$

The range of protons in aluminum is given by the semi-empirical formula

$$R_{Al}(\mu m) = \begin{cases} \dfrac{10.5E_p^2}{0.68 + 0.434\ln(E_p)} & 2.7MeV \le E_p \le 20MeV \\ 14.21E_p^{1.5874} & 1MeV < E_p \le 2.7MeV \end{cases} \tag{2.6}$$

For example, estimate the range of proton 3 MeV in air

$$R_{air}(m) = \left[\frac{E_p(MeV)}{9.3}\right]^{1.8} = \left[\frac{3}{9.3}\right]^{1.8} = 0.130\,m$$

Nowadays, some computer software is available for the calculation of stopping power and range of charged particles in different media. The most well-known one is the *SRIM (Stopping and Range of Ions in Matter)* program developed by Ziegler et al.

A series of such measurements with different charged particles and different energies is used to define the registration properties of a substance (Fleischer et al., 1964a; 1967a). For example, Figure 2.3 gives theoretical curves of the relative damage caused by different ions as a function of their velocities. The figure indicates the wide variation response, which extends from cellulose nitrate, which will register low energy proton (Jones and Neidigh, 1967) to those of minerals so insensitive that they will not register argon even at its maximum ionization rate (Fleischer et al., 1966; 1967b) [3].

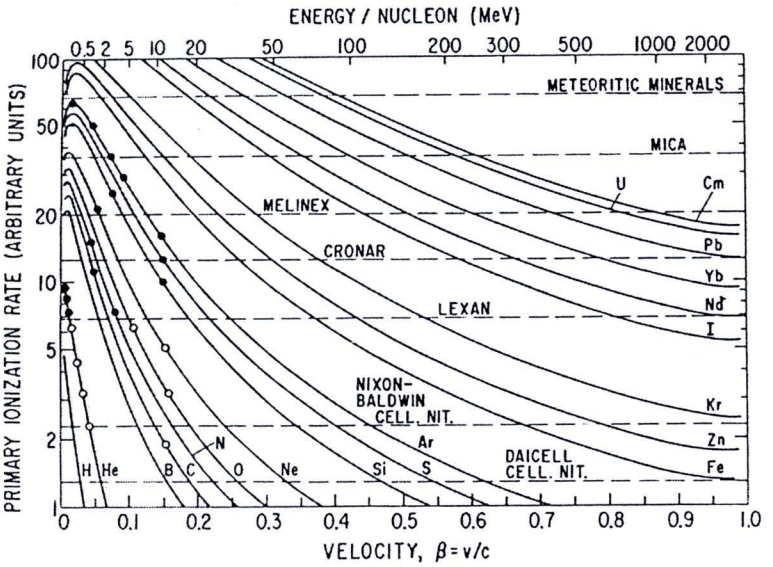

Figure 2.3 Damage vs. velocity for different charged particles. [3]

Each detector has a level below which no tracks are etched and one above which all particles create tracks. The experimental points for accelerator ions in Lexan polycarbonate are given as open circles for zero registration and as filled circles for 100% registration. Thresholds for other detectors are also indicated [3].

SSNTD materials can be ranked in order of sensitivity. Tables 2.2 and 2.3 are adapted from the compilation of Fleischer *et al.* [3]. They list a range of different materials and indicate for each the smallest ion that has been observed to form an etchable track, together with the energy of that ion. It is important to note that the data for polymers is often specific to a particular formulation and particles which form tracks in, say, one cellulose nitrate product may have no effect on a nominally similar polymer from a different manufacturer. In addition, registration behavior can be markedly influenced by etching conditions, for example, temperature, concentration, preconditioning by exposure to specific environments such as ultraviolet light and oxygen. Accordingly some overlap between closely ranked detector materials may occur when these experimental parameters are varied.

Table 2.2 Sensitivity order of track detector materials ranked in qualitative classes [2]

Organic SSNTDs (polymeric)

Material	Composition principal repeating unit(s)	Smallest ionizing ion detected (together with its energy where known)
Polyethylene	$[CH_2]_n$	
Polystyrene	$[CH_2\ CH\ C_6H_5]_n$	Fragments from fission processes
Polyvinylchloride–vinylacetate co-polymer	$\left[\begin{matrix}CH_2-CH\\ \quad\ Cl\end{matrix}\right]_n-\left[\begin{matrix}CH_2\ CH\\ \quad\ COOCH_3\end{matrix}\right]_m$	42 MeV ^{32}S
Polyvinylchloride–vinylidenechloride co-polymer	$\left[\begin{matrix}CH_2-CH\\ \quad\ Cl\end{matrix}\right]_n-\left[\begin{matrix}CH_2-C\ Cl_2\end{matrix}\right]_m$	42 MeV ^{32}S
Polyethylene	$[OC-C_6H_4-COO(CH_2)_2O]_n$	
Polyimide	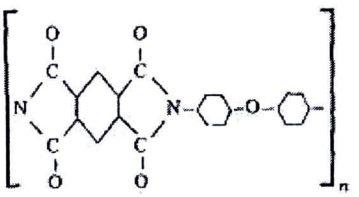	36 MeV ^{16}O
Polyoxymethylene	$[-CH_2O-]_n$	28 MeV ^{11}B
Polypropylene	$\left[\begin{matrix}CH_2-CH\\ \quad\ CH_3\end{matrix}\right]_n$	1 MeV ^4He
Polyvinylchloride	$\left[\begin{matrix}CH_2-CH\\ \quad\ Cl\end{matrix}\right]_n$	
Polymethylmethacrylate	$\left[\begin{matrix}CH_2-C.CH_3\\ \quad\ COOCH_3\end{matrix}\right]_n$	3 MeV ^4He
Cellulose esters	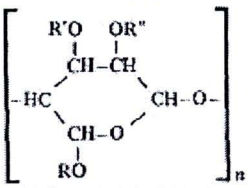 general structure	3 MeV ^4He
Cellulose acetate butyrate	where R = acetyl, R' = butyrate	
Cellulose triacetate	where R, R', R'' = acetyl	
Cellulose nitrate	where R = nitrate	0.55 MeV ^1H

Table 2.3 Inorganic SSNTDs (minerals, crystals, glasses) [2]

Material	Composition	Smallest ionizing ion detected and its energy
Diopside	$CaMg(SiO_3)_2$	170 MeV ^{56}Fe
Augite	$CaMg_3Fe_3Al_2Si_4O_{19}$	170 MeV ^{56}Fe
Hypersthene	$Mg_{1.5}Fe_{0.5}Si_2O_6$	100 MeV ^{56}Fe
Olivene	$MgFeSiO_4$	
Orthoclase	$KAlSi_3O_8$	100 MeV ^{40}Ar
Quartz	SiO_2	100 MeV ^{40}Ar
Soda-lime glass	$23SiO_2 : 5Na_2O : 5CaO : Al_2O_3$	20 MeV ^{20}Ne
Phosphate glass	$10P_2O_5 : 1.6BaO : Ag_2O : 2K_2O : 2Al_2O_3$	
Silica glass	SiO_2	16 MeV ^{40}Ar
Oligoclase	$Na_4CaAl_6Si_{14}O_{40}$	4 MeV ^{28}Si
Bytownite	$NaCa_6Al_9Si_{11}O_{40}$	4 MeV ^{28}Si
Phlogopite mica	$KMg_2Al_2Si_3O_{10}(OH)_2$	
Muscovite mica	$KAl_3Si_3O_{10}(OH)_2$	2 MeV ^{20}Ne
Labrodorite	$Na_2Ca_3Al_8Si_{12}O_{40}$	
Zircon	$ZrSiO_4$	
Bronzite	$Mg_{1.7}Fe_{0.3}Si_2O_6$	
Enstatite	$MgSiO_3$	
Flint glass	$18SiO_2 : 4PbO : 1.5Na_2O : K_2O$	2–4 MeV ^{20}Ne
Tektite glass (obsidian)	$22SiO_2 : 2Al_2O_3 : FeO$	

2.1.4 Categories of track-etched detector

Etchable tracks are formed in a variety of materials. All are electrical insulators, although some wide band gap semiconductors are also known to record tracks. The materials falls into two main categories: inorganic solids such as crystals and glasses, and organic solids, such as polymers. In the first category, the most popular materials are mica and flint glass, whereas polycarbonate and polyester films are the most common organic track-etch detectors. A list of the most useful materials is given in Table 2.4.

Table 2.4 The categories of track-etch detector [6]

Commonly Used track etch materials		
	Atomic Composition	Least Ionizing Ion Seen
Inorganic Materials		
Quartz	SiO_2	100 MeV ^{40}Ar
Phlogopite mica	$KMg_2Al_2Si_3O_{10}(OH)_2$	
Muscovite mica	$KAl_3Si_3O_{10}(OH)_2$	2 MeV ^{20}Ne
Silica glass	SiO_2	16 MeV ^{40}Ar
Flint glass	$18SiO_2:4PbO:1.5NaO_2:KO_2$	2-4 MeV ^{20}Ne
Organic Materials		
Polyethylene terephthalate (Cronar, Melinex)	$C_5H_4O_2$	36 MeV ^{16}O
Bisphenol A-polycarbonate (Lexan, Makrofol)	$C_{16}H_{14}O_3$	0.3 MeV ^{4}He
Polymethylmethacrylate (Plexiglass, Lucite, Perspex)	$C_5H_8O_2$	3 MeV ^{4}He
Cellulose triacetate (Cellit, Triafol-T,Kodacel TA-401 unplasticized)	$C_3H_4O_2$	
Cellulose nitrate (Daicell)	$C_6H_8O_9N_2$	0.55 MeV ^{1}H

Figure 2.4 demonstrated fission tracks from the same source ^{252}Cf in a variety of materials which can be viewed in a light microscope after chemical etching.

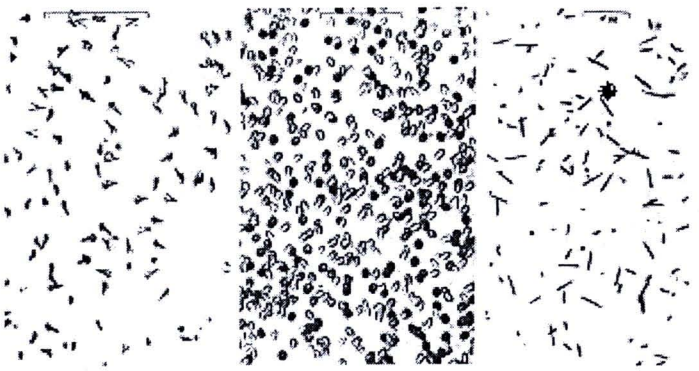

Figure 2.4 Drawings of etched fission tracks induced by the same source (^{252} Cf) in different materials: a) K feldspar; b) soda-lime glass; c) Lexan polycarbonate. [3]

2.2. Track etching

2.2.1. Track geometry [2]

The track can be made visible upon etching in a strong acid or base solution. The entire surface of the material is attacked, but those points at which particles tracks have entered are etched about 10 times faster. The tracks can thus be made to form pits on the surface that are large enough to be easily visible through an optic microscope.

The chemical action of the etch is characterized by the ratio V_T/V_G where V_T is the rate of dissolution along the track and V_G the bulk etch rate of the detector surface remote from any tracks (G ≡ general). In the simple instance of a particle penetrating a detector normal to its original surface as in Figure 2.4 and assuming that V_T is constant along the track and V_G is constant and isotropic, then V_T/V_G will be constant for short etching distances in isotropic non-crystalline solids. Both l and d are directly observable quantities from the competitive effects of V_G and V_T and become smaller as V_T approaches V_G and vice versa, i.e. both l and d decrease as V_T/V_G decreases. Hence, for the situation envisaged in Figure 2.5:

$$l = (V_T - V_G)t \tag{2.2}$$

where t = etching time, and

$$d = 2V_G t\left[\frac{(V_T - V_G)}{(V_T + V_G)}\right]^{1/2} \tag{2.3}$$

It can be seen that when $V_T = V_G$, both l and d vanish, which is a required property of these equations. Also the cone angle, as defined in Figure 2.5 is given by Eq. 2.4:

$$\theta = \sin^{-1}\left(V_G / V_T\right) \tag{2.4}$$

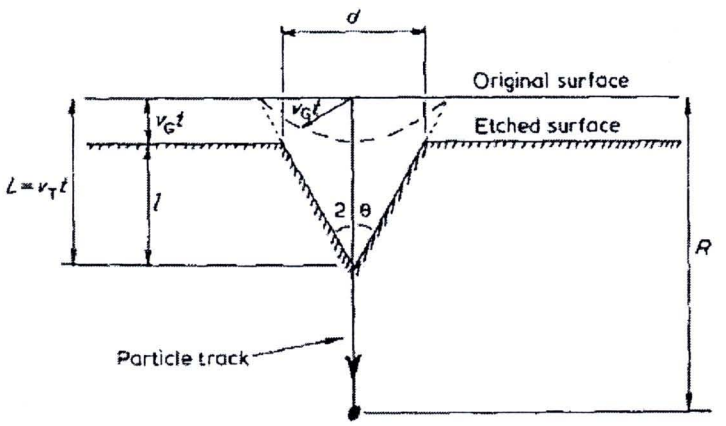

Figure 2.5 Track etching geometry with V_T and V_G constant for a vertically incident particle. [3]

The geometry of the etched track becomes more complicated if V_T varies along the track length, and this more realistic situation has been treated by Fleischer *et al.* In general terms, an increasing V_T with depth will produce a cone of increasing sharpness, the surfaces being concave from without, while a decreasing V_T will give the opposite effect, although the cone point remains sharp until V_T has decreased virtually to the bulk etch velocity of V_G.

For the more general case of oblique particle incidence, the geometry is more complicated. If track inclined with the track obliquity angle, ϕ at less than the critical angle θ_c to a surface can be erased by the etching process. (Figure 2.6) Then the incidence angle must exceed a critical angle in order to avoid its disappearance due to the progressive etching of the normal surface.

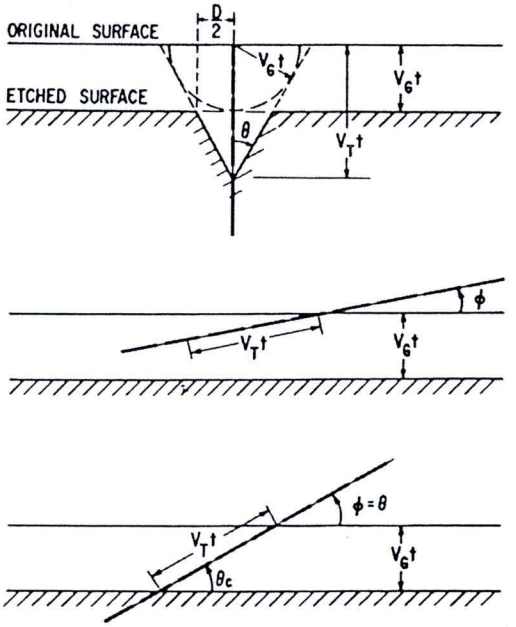

Figure 2.6 (a) Model of track etching in which the normal surface is removed at a velocity V_G and the damaged track at a velocity V_T, leading to a cone-shape pit.

(b) Tracks formed at an angle ϕ less than the critical angle θ_c are not revealed because the normal surface advances faster than the etch rate along the track.

(c) The case in which the particle enters at the critical angle θ_c. Tracks entering the surface at an angle greater than the critical angle will be visible after etching. [3]

2.2.2. Factors influencing etch rate

In principle, any chemical reagent will function as an etchant if it attacks a detector at an appropriate rate, and usually etching conditions are optimized empirically for each detector material. For minerals and glasses, many etchants are based on hydrofluoric acid and etchants for polymeric detectors are frequently solutions of alkali hydroxides.

The etch rate of nuclear track etch in certain SSNTD depends on the following;

a) The nature, concentration, and temperature of the etchant used.

b) The time of etching

c) The environmental conditions existing before, during and after irradiation.

There have been many investigations to study the etching parameters for the more common polymeric detectors. These have elucidated the influence of composition of the etchants, its strength, its temperature and also degree of liquid agitation and various pre-etching treatments on the development of track pits. Figure 2.7 and 2.8 are examples of this extensive data. [2]

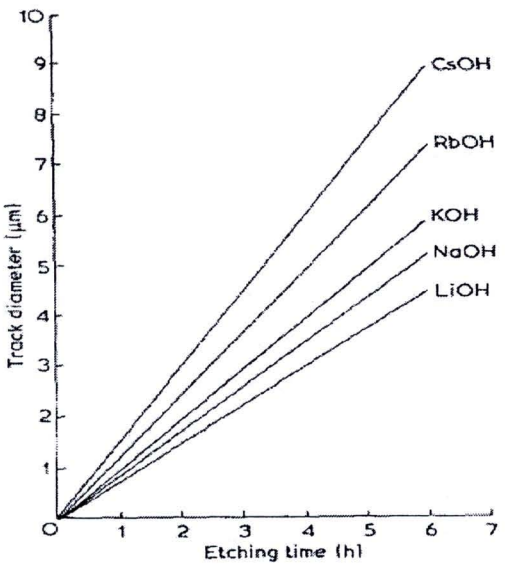

Figure 2.7 The effect of alkali hydroxide type on the track etching rate of a polycarbonate. 5N solution of 60°C. [2]

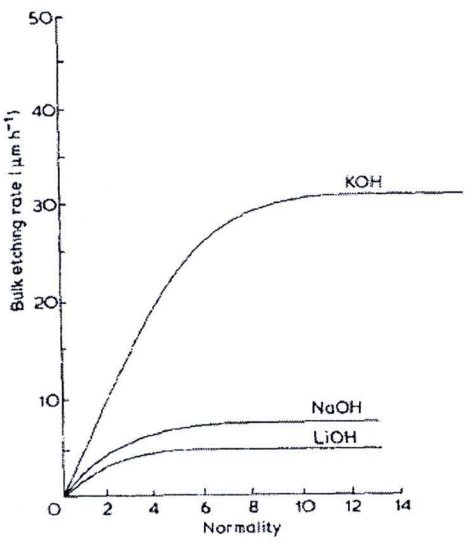

Figure 2.8 The effect of etchant concentration on the bulk etching rate of a cellulose nitrate detector (Daicell) at 50°C. [2]

Temperature and concentration of chemicals are variables that allow control of the attack rate so that etching occurs, but not too rapidly, as illustrated by Figure 2.9 [3].

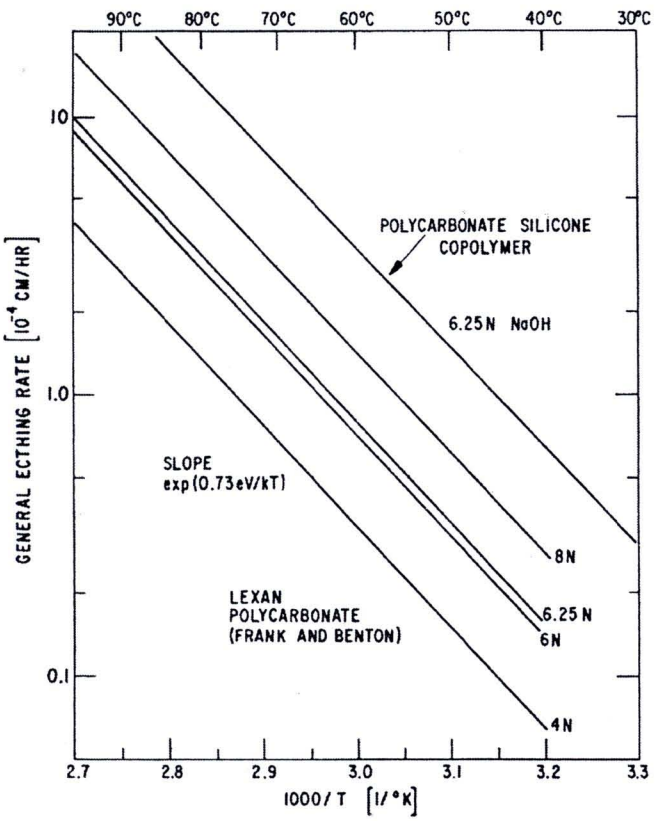

Figure 2.9 Etching rates are typically exponential functions of inverse temperature and increase with concentration. [3]

The shape of the track changes drastically with prolonged etching, going through three phases: conical, of transition, and spherical (see Figure 2.10). The final geometry of the etch pit profile depends, therefore, on the instant when the chemical etching is stopped. The conical phase lasts until the etching reaches the end of the damage trail. In this phase, the shape of the track is conical and its open surface is elliptical. When this phase finishes, the transition phase starts in which the bottom of the track is being rounded whereas the open surface is still elliptical. The etching rate is, then equal to the bulk etch rate in all directions. The spherical phase is reached when the shape of the track is spherical and its open surface circular [8].

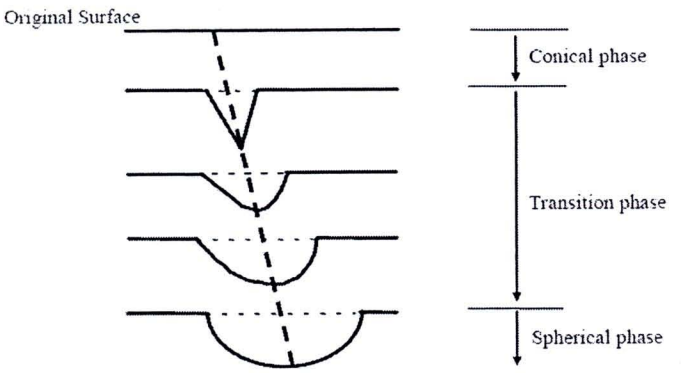

Fig. 2.10 The evolution of an etch pit profile with prolonged chemical etching. [8]

Polymer surfaces on exposure to photo-radiation undergo various changes, either alone or in combination, usually of oxidative, ozonolysis, or thermal character which causes chain scission and/or crosslinking. Such effects lead to either localized or bulk surface hardening, or softening, dependent on the dominant reaction in any specific instance. Surface "hardening", often caused by heating or ageing, is usually associated with a decrease in etching rate, while "softening" can cause a substantial increase. "Softening" agents observed, in addition to ultraviolet light have been O_3, H_2O_2 , NO. The moisture content of some detectors, as indicated by their storage humidity conditions, can also affect the etching rates of a water-sensitive polymer, e.g. cellulose nitrate can be made to double its etching rate. It has also been reported that the storage of polycarbonate in liquid nitrogen prior to etching increases its sensitivity to a particles.

A neutral environment of vacuum or nitrogen atmosphere decreases the track etching rate, possibly by oxygen exclusion. It is useful to note that the detector cellulose triacetate irradiated in a vacuum will not display alpha particle tracks on etching but can be sensitized after exposure to oxygen at high pressure (~ 100 atm).

Cellulose nitrates, polycarbonates, polyethylene terephthalate all show increased track etching rates on exposure to O_2, NO, H_2O_2 + ultraviolet light. Exceptionally, N_2O+ ultraviolet decreases track etching rates.

The experimental consequences of these facts are that polycarbonates, after irradiation, need protection from ultraviolet light sources such as sunlight and fluorescent lights if it is important that their track etching properties be standardized. Cellulosics after

either prompt processing, or refrigeration, to suspend any chemical changes as in this instance the etch rate slowly decreases with time and gradual polymer decomposition occurs.

The various additives, anti-degradients, plasticizers, etc., used in formulating polymer materials often considerably change their etching characteristics, rate variations of 1 to 35 have been reported. In particular, the presence of an ultraviolet stabilizer is recognized as suppressing the track-etching properties of polymeric detectors by conferring opacity to ultraviolet light.

In the case of crystalline materials, high doses of lightly ionizing radiation have so far failed to alter measurable etching parameters. However, weathering, specific annealing, and other thermal effects, do play influential roles in the etching of tracks in inorganic detectors [2].

Examples of some commonly used solid state nuclear track detectors are given in Table 2.5 [8]. A list of chemical etchants generally used along with the etching conditions for different detectors, particle sensitivity and the critical angle of etching are also given in Table.

Table 2.5 Examples of etching condition of SSNTDs. [11]

Category	Detector Material	General Etching Conditions	Lightest Detectable Particle	Critical Angle Q_c
Minerals/ Crystals	Olivine	KOH Soln., 160°C, 6 min; 10 % HF, 23°C, 30 sec.	Fe	
	Zircon	85 % H_3PO_4, 500°C, 1 min.	Ca	
	Quartz	KOH Soln., 210°C, 10 min.	Ar (100 MeV)	
	Mica	48 % HF, 23°C, 3 Sec- 40 min.	Ne(20 MeV)	4° 30′
Glasses	Sodalime glass	48 % HF, 23°C, 3 Sec.	Ne(20 MeV)	~ 50°
	Phosphate glass	48 % HF. 23°C, 3 Sec.	F (20 MeV)	1-5°
Plastics	Polycarbonate Plastics (Lexan, Makrafol, Milar)	6 N NaOH, 60°C, 60 min.	He (0.3 MeV)	~ 2-3°
	Cellulose Nitrate (Daicell, LR-115, CA-80-15)	3-6N NaOH, 50°C, 40 min.	H (0.5 MeV)	~ 4-8°
	Allyldiglycol Polycarbonate (CR-39)	6 N NaOH, 70°C, 1-4 hrs.	H (1.0 MeV)	~ 10°

For a clear concept and practical use of the track formation phenomena one must predict that at how much energy particles will produce etchable tracks under certain fixed

experimental conditions. Various scientists have suggested that track formation should be related to number of different parameters. For an exact and precise analysis of track formation phenomena, some of the important parameter taken into account is the following

i) Charge, mass and velocity of the traversing ion.

ii) The typical critical angle θ with respect to surface of the detector.

iii) Types of the detector material.

iv) Nature, concentration, and temperature of the etchant

v) Etching time

vi) Environmental conditions existing before, during and after irradiation.

2.3. Applications of Track-etched detectors

The areas of potential applications of Solid State Nuclear Track Detectors are growing rapidly. In 2006, P. Buford Price [4] had brief reviews of applications of the nuclear track technique to nuclear fusion, cosmic rays, molecular identification with nanopores, imaging X-ray astronomy, magnetic studies with nanowires, polymeric nanowires, radon and neutron dosimetry, and thermochronology with ^{238}U and ^{244}Pu fission tracks. These are some applications of filtering from his reviews.

2.3.1 Research and technology with nanopores in track-etch films

DeBlois and Bean (1970) and co-workers (DeBlois and Wesley, 1977; DeBlois et al., 1977), who used a single track-etched pore in a polycarbonate film to detect and measure sizes of viruses down to ~40 nm.

In 1991 David Deamer (U. C. Santa Cruz) and Daniel Branton (Harvard) initiated research on nanopore sequencing of single-stranded nucleic acids. They and their colleagues hit upon the idea of using a cage-like molecule, α-hemolysin, containing a pore with an internal diameter of ~2.2 nm and a limiting aperture of 1.5 nm diameter. This pore can be embedded in a lipid bilayer and an electrical field used to drive a single strand of a charged DNA fragment through the pore. Although such membranes have been successful in measuring long stretches of the same nucleotides, such as 30 adenines followed by 70 cytosines (Kasianowicz et al., 1996; Akeson et al., 1999), current research is aimed at identifying each nucleotide as it passes through the pore. One of

Deamer's ideas is to use mica with a 6 nm single pore to support an α-hemolysin pore and to slow the rate of passage of nucleic acid fragments to ~10^{-3} sec per base in order to avoid blurring of signals. There is now considerable effort, especially among those who use the Unilac heavy ion facility at Darmstadt, Germany, to develop synthetic nanopores small enough to compete with α- hemolysin. Mara et al. (2004) have made a good start, using asymmetric pores 2 to 4 nm in diameter in a polyimide film to distinguish double-strand DNA fragments in the size range from ~290 to ~4000 base pairs. Heins et al. (2005) have recently shown that a conically shaped polyimide film with a single 4.5 nm nanopore is able to detect single porphyrin molecules of diameter ~2 nm.

2.3.2 Ion track filters for imaging X-ray astronomy

Mitrofanov and Apel (2006) have developed a blocking cut-off filter that rejects UV and visible light from the sun while allowing soft X-rays to penetrate the film. Three identical filters capable of rejecting the 10^8-times larger flux of solar UV and visible light have been installed in the SPIRIT telescope assembly, which includes a Herschel telescope-coronagraph and a Ritchey- Chrétien telescope that have been operating on board the Coronas-F satellite since 2001. The filter used is an 8.5-μm-thick PET foil with a density of 1.4 x 10^7 cm^{-2} etched tracks of diameter 1.5 μm and with two-layer thin Al films on each surface. It was optimized for detection of 13.5 to 30.4 nm X-rays. The UV and visible light is cut off by diffraction and absorption on the pore walls.

2.4 Neutron Interactions [12, 13]

Since neutrons are electrically neutral, they are not affected by the electrons in an atom or by the positive charge of nucleus. As a consequence, neutron passes through the atomic electron cloud and interacts directly with the nucleus. In short, neutrons collide with nuclei, not with atoms. A neutron can have many types of interactions with a nucleus. Figure 2.11 shows the types of interactions.

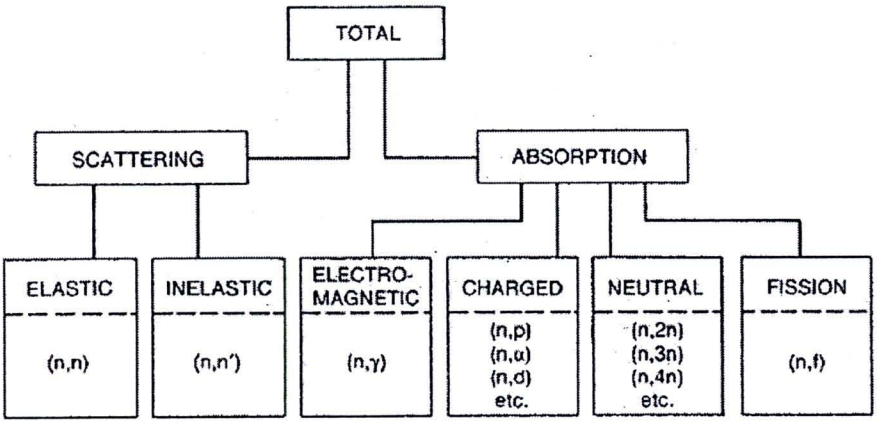

Figure 2.11 Various categories of neutron interactions. The letters separated by commas in the parentheses show the incoming and outgoing particles. [13]

An interaction may be one of two major types scattering or absorption. When a neutron is scattered by a nucleus, its speed and direction change but the nucleus is left with the same number of protons and neutrons it had before the interaction. The nucleus will have some recoil velocity and it may be left in an excited state that will lead to the eventual release of radiation. When a neutron is absorbed by a nucleus, a wide range of radiations can be emitted or fission can be induced.

2.4.1 Elastic scattering

In this process, the neutron strikes the nucleus, which is almost always in its ground state, the neutron reappears, and the nucleus is left in its ground state. The neutron in this case is said to have been elastically scattered by the nucleus. In the notation of nuclear reactions, this interaction is abbreviated by the symbol (n,n).

2.4.2 Inelastic scattering

This process is identical to elastic scattering except that the nucleus is left in an excited state. Because energy is retained by the nucleus, this is clearly an endothermic interaction. Inelastic scattering is denoted by the symbol (n,n').

2.4.3 Electromagnetic or Radiative Capture

Here the neutron is captured by the nucleus, and one or more γ rays – called capture γ rays- are emitted. This is an exothermic interaction and is denoted by (n,γ). Since the original neutron is absorbed, this process is an example of a class of interactions known as absorption reactions.

2.4.4Charged Particle Reaction

Neutrons may also disappear as the result of absorption reactions of the type (n,α) and (n,p). Such reactions may be either exothermic or endothermic.

2.4.5 Neutron producing reactions

Reactions of the type (n,2n) and (n,3n) occur with energetic neutrons. These reactions are clearly endothermic since in the (n,2n) reaction one neutron and in the (n,3n) reaction 2 neutrons are extracted from the struck nucleus.

2.4.6 Fission

Neutrons colliding with certain nuclei may cause the nucleus to split apart- to undergo fission.

2.5 Theory of Light [14]

Light is just one portion of the various electromagnetic waves (Figure 2.12). The electromagnetic spectrum covers an extremely broad range, from radio waves with wavelengths of a meter or more, down to x-rays with wavelengths of less than a billionth of a meter. Optical radiation lies between radio waves and x-rays on the spectrum, exhibiting a unique mix of ray, wave, and quantum properties.

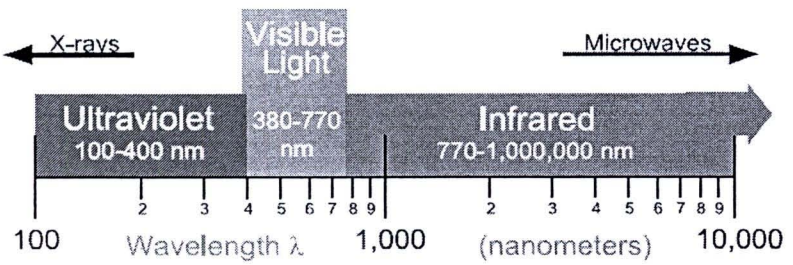

Figure 2.12 The optical portion of the electromagnetic spectrum. [14]

Like all electromagnetic waves, light waves can interfere with each other, become directionally polarized, and bend slightly when passing an edge. These properties allow light to be filtered by wavelength or amplified coherently as in a laser.

In radiometry, light's propagating wavefront is modeled as a ray traveling in a straight line. Lenses and mirrors redirect these rays along predictable paths. Wave effects are insignificant in an incoherent, large scale optical system because the light waves are randomly distributed and there are plenty of photons.

2.5.1 Ultraviolet Light

Short wavelength UV light exhibits more quantum properties than its visible and infrared counterparts. Ultraviolet light is arbitrarily broken down into three bands, according to its anecdotal effects (Figure 2.13). UV-A is the least harmful and most commonly found type of UV light, because it has the least energy. UV-A light is often called black light, and is used for its relative harmlessness and its ability to cause fluorescent materials to emit visible light - thus appearing to glow in the dark. Most phototherapy and tanning booths use UV-A lamps.

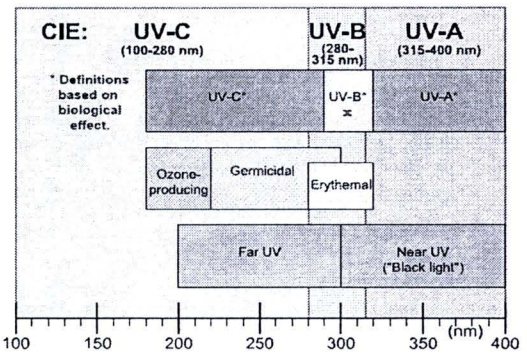

Figure 2.13 Common ultraviolet band designations. [14]

UV-B is typically the most destructive form of UV light, because it has enough energy to damage biological tissues, yet not quite enough to be completely absorbed by the atmosphere. UV-B is known to cause skin cancer. Since most of the extraterrestrial UV-B light is blocked by the atmosphere, a small change in the ozone layer could dramatically increase the danger of skin cancer. Short wavelength UV-C is almost completely absorbed in air within a few hundred meters. When UV-C photons collide with oxygen atoms, the energy exchange causes the formation of ozone. UV-C is almost never observed in nature, since it is absorbed so quickly. Germicidal UV-C lamps are often used to purify air and water, because of their ability to kill bacteria.

2.5.2 Visible Light

Visible light ranges in wavelength from approximately 400 nm to 700 nm. It is also known as the optical spectrum of light. The wavelength (which is related to frequency and energy) of the light determines the perceived color. The ranges of these different colors are listed in the Table 2.6 below. Some sources vary these ranges pretty drastically, and

the boundaries of them are somewhat approximate as they blend into each other. The edges of the visible light spectrum blend into the ultraviolet and infrared levels of radiation.

Table 2.6 The Visible light spectrum

The Visible light Spectrum	
Color	Wavelength (nm)
Red	625 - 740
Orange	590 - 625
Yellow	565 - 590
Green	520 - 565
Cyan	500 - 520
Blue	435 - 500
Violet	380 - 435

Most light that we interact with is in the form of *white light*, which contains many of these entire wavelength ranges within them. Shining white light through a prism causes the wavelengths to bend at slightly different angles due to optical refraction. The resulting light is, therefore, split across the visible color spectrum.

2.5.3 Infrared Light

Infrared light contains the least amount of energy per photon of any other band (Figure 2.14). Because of this, an infrared photon often lacks the energy required to pass the detection threshold of a quantum detector. Infrared is usually measured using a thermal detector such as a thermopile, which measures temperature change due to absorbed energy.

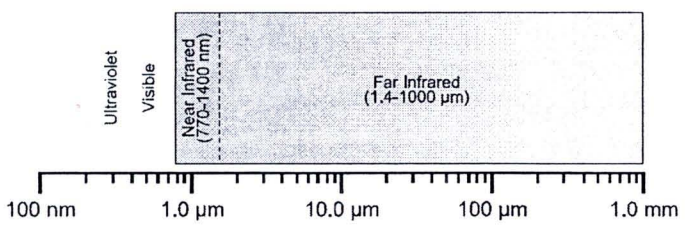

Figure 2.14 The infrared spectrum. [14]

While these thermal detectors have a very flat spectral responsivity, they suffer from temperature sensitivity, and usually must be artificially cooled. Another strategy employed by thermal detectors is to modulate incident light with a chopper. This allows the detector to measure differentially between the dark (zero) and light states.

Quantum type detectors are often used in the near infrared, especially below 1100 nm. Specialized detectors such as InGaAs offer excellent responsivity from 850 to 1700 nm. Typical silicon photodiodes are not sensitive above 1100 nm. These types of detectors are typically employed to measure a known artificial near-IR source without including long wavelength background ambient.

Since heat is a form of infrared light, far infrared detectors are sensitive to environmental changes - such as a person moving in the field of view. Night vision equipment takes advantage of this effect, amplifying infrared to distinguish people and machinery that are concealed in the darkness.

Infrared is unique in that it exhibits primarily wave properties. This can make it much more difficult to manipulate than ultraviolet and visible light, infrared is more difficult to focus with lenses, refracts less, diffracts more, and is difficult to diffuse. Most radiometric IR measurements are made without lenses, filters, or diffusers, relying on just the bare detector to measure incident irradiance.

2.5.4 Behavior of Light

The behavior of light pass through the matter can be divided to

2.5.4.1 Reflection

Reflection is the change in direction of a wavefront at an interface between two different media so that the wavefront returns into the medium from which it originated. Light reflecting off of a polished or mirrored surface obeys the law of reflection: the angle between the incident ray and the normal to the surface is equal to the angle between the reflected ray and the normal (Figure 2.15). When light obeys the law of reflection, it is termed a specular reflection. Most hard polished (shiny) surfaces are primarily specular in nature. Even transparent glass specularly reflects a portion of incoming light.

Many reflections are a combination of both diffuse and specular components. One manifestation of this is a spread reflection, which has a dominant directional component that is partially diffused by surface irregularities (Figure 2.16).

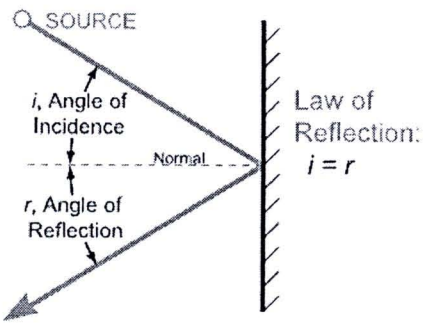

Figure 2.15 Law of reflection. [14]

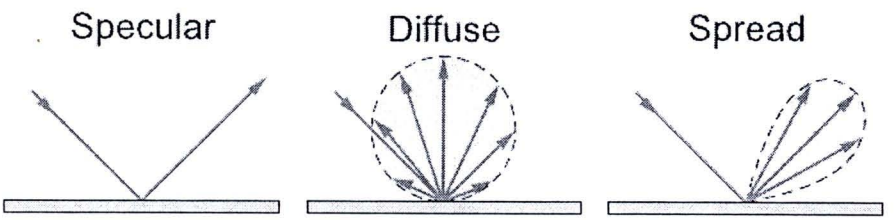

Figure 2.16 Specular, diffuse, and spread reflection from a surface. [14]

2.5.4.2 Refraction

When light passes between dissimilar materials, the rays bend and change velocity slightly, an effect called refraction (Figure 2.17). Refraction is dependent on two factors: the incident angle, θ_1, and the refractive index, n of the material, as given by Snell's law of refraction:

$$n_1 \sin(\theta_1) = n_2 \sin(\theta_2) \quad (2.6)$$

where: n_1 is the refractive index of the medium the light is leaving,

$\theta 1$ is the incident angle between the light ray and the normal to the medium to medium interface,

n_2 is the refractive index of the medium the light is entering,

$\theta 2$ is the refractive angle between the light ray and the normal to the medium to medium interface

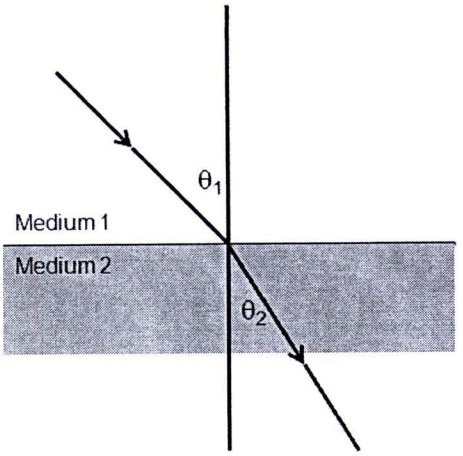

Figure 2.17 Refraction of light.

2.5.4.3 Diffraction

Diffraction is another wave phenomenon that is dependent on wavelength. Light waves bend as they pass by the edge of a narrow aperture or slit (Figure 2.18). This effect is approximated by:

$$\theta = \lambda / D \qquad (2.7)$$

where θ is the diffraction angle, λ the wavelength of radiant energy, and D the aperture diameter. This effect is negligible in most optical systems, but is exploited in monochromators. A diffraction grating uses the interference of waves caused by diffraction to separate light angularly by wavelength. Narrow slits then select the portion of the spectrum to be measured. The narrower the slit, the narrower the bandwidth that can be measured. However, diffraction in the slit itself limits the resolution that can ultimately be achieved.

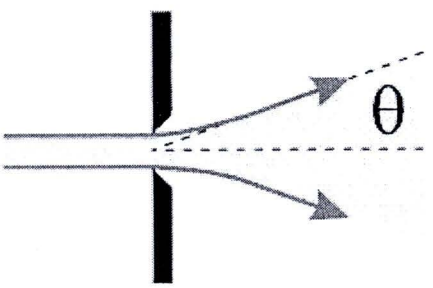

Figure 2.18 Diffraction of light. [14]

2.5.4.4 Transmission

When a beam monochromatic light passes through a transparent medium, part of the light is absorbed and the transmitted beam has a lower intensity than the intensity of the incident beam. The light that does not get through is said to be absorbed by the medium through which it passes.

Absorption by a filter glass varies with wavelength and filter thickness. Bouger's law states the logarithmic relationship between internal transmission at a given wavelength and thickness.

$$Log_{10}(\tau_1) / d_1 = log_{10}(\tau_2) / d_2 \qquad (2.8)$$

Internal transmittance, τ_1, is defined as the transmission through a filter glass after the initial reflection losses are accounted for by dividing external transmission, τ_2 by the reflection factor Pd.

$$\tau_1 = T / Pd \qquad (2.9)$$

When light passes through the rough material, it is often necessary to diffuse light, either through transmission or reflection (Figure 2.15). Diffuse transmission can be accomplished by transmitting light through roughened quartz, flashed opal, or polytetrafluoroethylene (PTFE, Teflon). Diffusion can vary with wavelength. Teflon is a poor IR diffuser, but makes an excellent visible/UV diffuser. Quartz is required for UV diffusion. Integrating spheres are coated with $BaSO_4$ or PTFE, which offer >97% reflectance over a broad spectral range with near perfect diffusion. These coatings are, however, quite expensive and fragile. It is often necessary to diffuse light, either through transmission or reflection.

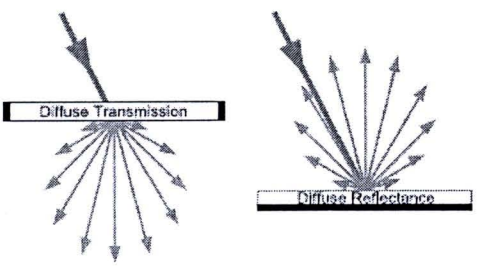

Figure 2.19 Diffuse transmission and reflectance. [14]

In 2007, Ali Mostofizadeh, Xiudong Sun and Mohammad Reza Kardan [15] reviewed paper to summarize some advanced theoretical and experimental methods applied in modern optics to develop some technical skills used in nuclear track studies. One of his reviews mentioned that some researcher using optical model about light transmission and light scattering phenomenon to describe the optical properties on nuclear track. Grietz et al., 1998 explained about light scattering phenomenon by conical and oblique etched track has been schematically shown in figure 2.16 and 2.17

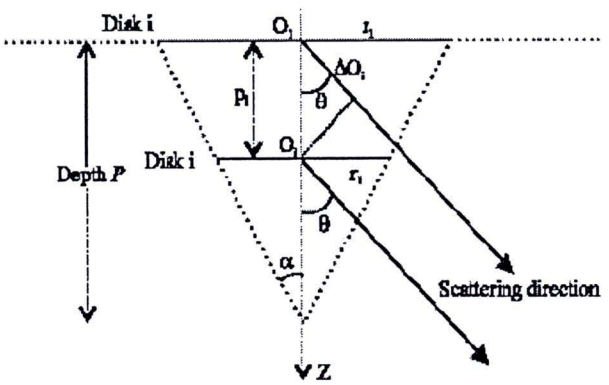

Figure 2.20 Geometry of a conical. [15]

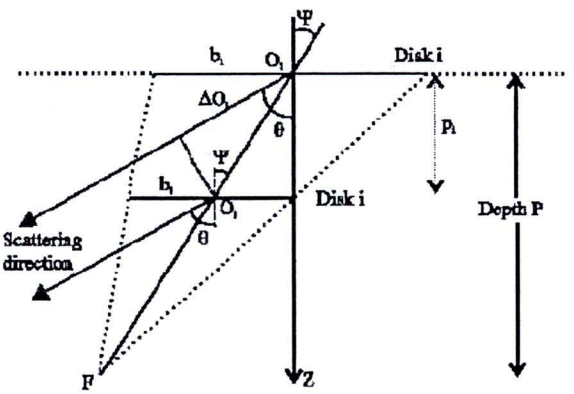

Figure 2.21 Geometry of an oblique tracks. [15]

His reviews mentioned about neutron and alpha particles etched tracks evaluation using He-Ne laser. Al-Saad et al. (2001) attempted to apply He-Ne laser light to investigate nuclear tracks of ^{241}Am alpha particles and Am-Be neutrons, registered by 250 μm CR-39 and 100 μm CN-85 foils. They used a photodiode as a light detector at the

distance 10 cm from the SSNTDs for measuring light scattered by track apertures. Figure 2.18 and showed the behavior of light transmission through the CR-39 and CN-85 foils irradiated by alpha particles and neutron in the normal incidence case (0^{o}) versus chemical etching time, respectively.

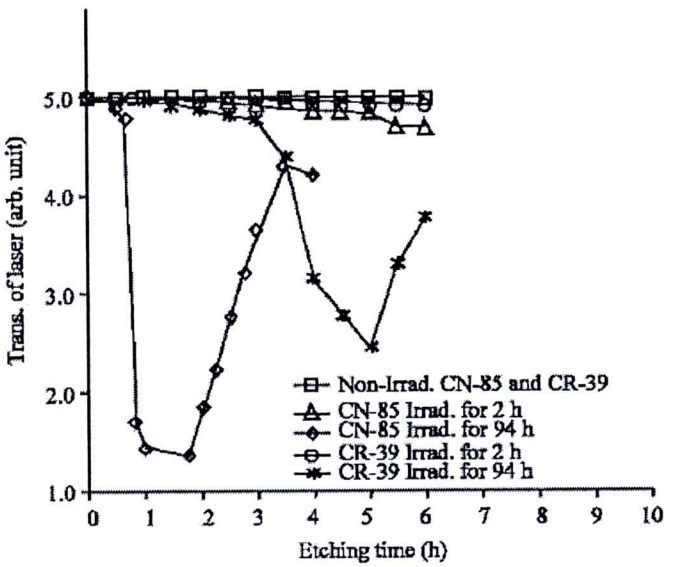

Figure 2.22 Transmission of laser light through the SSNTD's irradiated by α particle. [15]

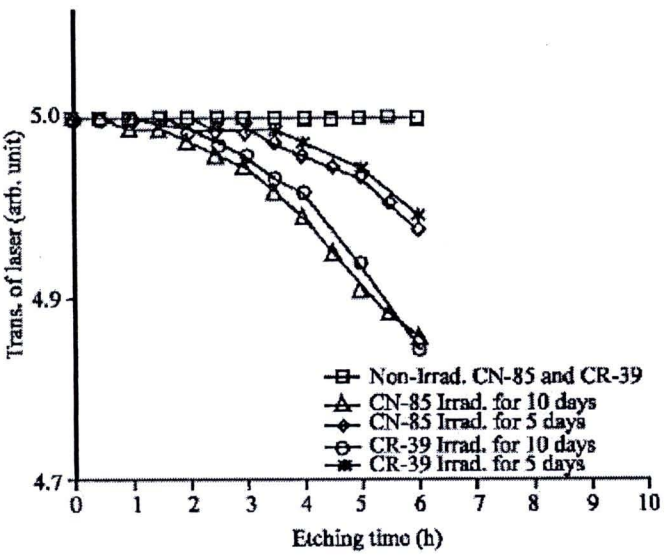

Figure 2.23 Transmission of laser light through the SSNTD's irradiated by neutron. [15]

The pattern of transmission of laser light through the SSNTD' irradiated by neutron is different from SSNTD' irradiated by alpha particle. They stated that the different

mechanism to generate fast-neutron-induced tracks in polymers can cause a different feature for mention curves. Since nuclear tracks are in fact the particular damages in polymeric structure of SSNTDs that are created by charge particles, neutrons (as electrical neutral particles) cannot directly be able to create primary latent tracks. Nonetheless, tracks are indirectly induced by neutrons based on creating of charged induced recoil-particles in the polymeric structure. On the other hand, the productive reactions of recoil-particles can occur anywhere inside the polymer volume along the neutrons trajectory, so there is no necessarily that the related polymeric destruction begins from the surface of polymer. Therefore, new tracks are likely to be created due to increase of etching time.

In this study, random and asymmetric track-etch pores in polymer used as light filter or diffuser films are generated by neutron induced track-etch. Neutrons from radioisotope source interact with hydrogen or nitrogen atoms of polymer via $^{1}H\ (n,n)^{1}H$ and $^{1}H\ (n,n')^{1}H$. Proton tracks will be created on polymer. Their pore size and shape can be varied in controllable manner which involve the temperature, the concentration of the etchant, and the etching duration.

2.6 Literature review

In 1975, Nares Chankow [16] used Cellulose nitrate (CN) to register radon alpha particles which diffused from uranium ore. In this study, he also varied the etching condition. He found that the optimum etching conditions used were 10% solution of NaOH, 60°C and 40 minutes etching time. And the alpha track densities on the films were proportional to the amount of uranium and radium in the ore.

In 1981, Stephens, Richard B. [17] patented about low reflectivity surfaces which are formed by particle track etching of a dielectric material such that the horizontal scale of surface texture is less than the wavelength of incident radiation and the depth of texture is equal to or greater than said wavelength. As a consequence, the reflection coefficient is thereby reduced by a factor of at least two, and light is more efficiently transmitted into the material. For solar cells encapsulated in transparent material, efficiency of absorption of solar radiation may be improved by at least about two times per etched surface, or to less

than about 2% for the air/transparent material interface and to less than about 15% for the transparent material/solar cell interface.

In 1989, Hameed Ahmed Khan and Naeem Ahmed Khan [18] had a review article Solid State Nuclear Track detection (SSNTD): A useful scientific tool for basic and applied research. In this paper, very briefly, summarizes the useful contribution this technique has made in the past and is making at present. The state of the art of applications of Solid State Nuclear Track Detectors in fields like nuclear physics, geochronology, cosmology, biology, bird altimetry, seismology, elemental analysis, material science, lithography, etc. has been given.

In 1991, Michael A. Gruntman [19] reviewed a novel of the filtering of EUV radiation for laboratory and space applications. The relevant theoretical considerations as well as available experimental data are presented. Foils perforated by a set of parallel channels with submicron diameters serve as wavelength dependent filters. Each channel passes photons when the wavelength is much smaller than the channel diameter. The transmission of the channel drops dramatically, however, when the wavelength becomes comparable to or larger than the channel diameter. Several different ways to manufacture such kind of filters are outlined, including nuclear track filters, anodized metal films, and microchannel plate technology. Advantages and disadvantages of each technique are discussed.

In 1996, P. C. Popov and D. S. Pressyanov [20] exposed Kodak-Pathe' LR 115 type II, at 25 mm distance, to alpha particles of a spectrometric ^{238}Pu source. After that the detectors were etched in 10% NaOH at 60°C for 120 min. The estimation of track densities is within 103-105 cm^{-2} range. A modified SSNTD is placed in optical contact with a prism, so that sensitive surface of the detector faced the microscope, to assess the internal reflection of a laser beam. They concluded that it can be obstructed total internal reflection of a laser beam.

In 2001, Nares Chankow, et al. [21] developed a technique for viewing Track-Etch neutron radiographs using a desktop scanner with a nickel coated metal backing which was placed on the scanner. It was found to be practical in viewing track-etch neutron radiographs without any additional development or investment.

In 2006, A.V. Mitrofanov, P.Yu. Apel [22] applied ion track filters as blocking cut-off filters for solar telescopes in imaging X-ray astronomy. Ion track membranes (ITMs) were produced of polyethylene terephthalate (PET) foils with the thickness L of 5–25 μm. Specimens of the PET foils were irradiated with the 250 MeV Kr ions up to the track density N of 10^6– 10^8 cm^{-2} on the U-400 cyclotron of the Flerov Laboratory of Nuclear Reactions JINR. ITms of high-porosity constitute a randomly inhomogeneous medium with sub-micrometer or micrometer open pores which not only transmits X-ray or extreme ultra violet (EUV) radiation and blocks long-wavelength UV radiation, but also transfers a focused imaging pattern with high-quality for further registration by means of CCD or imaging detectors of other types. X-ray and EUV filters based on ITMs with cylindrical parallel pores were successfully used as detector filters in the solar X-ray telescopes designed and manufactured at the Lebedev Physical Institute of the Russian Academy of Sciences (LPI, Moscow).

In 2006, A. V. Mitrofanov, P. Yu. Apel, I. V. Blonskaya and O. L. Orelovitch [23] found experimentally that porous polyimide and poly (ethylene naphthalate) membranes made by chemical etching of ion tracks using a scanning beam of 253-MeV ^{84}Kr ions on the U-400 cyclotron (Flerov laboratory, Joint Institute of Nuclear Research) are promising for optical diffraction filters and supports of thin-film filters used in X-ray astronomy instruments and also for laboratory applications. A series of large-pore membranes was fabricated from PI and PEN films, and their parameters were measured. These membranes may be used as components of neutral-density optical filters in the soft X-ray and vacuum ultraviolet spectral ranges.

In 2007, Ali Mostofizadeh, Xiudong Sun and Mohammad Reza Kardan [13] reviewed to summarize some advanced theoretical and experimental methods applied in modern optics to develop some technical skills used in nuclear track studies. They also described the process of tracks appearance in solid state detectors, the theoretical principles of light transmission through the polymeric detectors, some features of Fourier optics, practical and experimental aspects of the subject including the applications of coherent light in nuclear track evaluations.

In 2007, D. Nikezic and K.N. Yu [5] used a computer program called TRACK_VISION 1.0 which was developed in their laboratory to simulate light propagation

through the tracks and to calculate the brightness of all grid elements in the track wall. Four different cases for light ray propagation through the etched track were studied in detail. The track profile, optical appearance and distribution of scattered light were given for three typical types of etched tracks. These laid the foundation for future automatic determination of properties of the alpha particles producing the tracks through the scattered light.

In 2008, D. Nikezic and K.N. Yu [24] continued their works about a computer program called Track_Vision for determining the optical appearances of tracks in nuclear track materials. Their programming steps were outlined. This paper described the program were given, including the built-in *V* functions for the commonly employed nuclear track material commercially known as CR-39 (polyallyldiglycol carbonate) irradiated by alpha particles.